APPLIED GEOPHYSICS, Vol.14, No.2 (June 2017), P. 314–321, 5 Figures.
DOI:10.1007/s11770-017-0622-0

Regional spatiotemporal variations of a nondipole magnetic field over the Chinese mainland and neighboring regions in millennial scale*

Feng Yan♦[1,2] and Jiang Yong[1]

Abstract: Spatiotemporal variations of the nondipole (ND) magnetic field over the Chinese mainland and neighboring regions from 10000 BC to 1990 AD were analyzed using the latest global geomagnetic models CALS10K.1b, CALS3K.4, and IGRF11. Moreover, for field sources, we investigated 2^n (n = 2–10) pole ND fields and their energies. The results suggest that the study period can be divided into three. The intensity of the ND field has been mainly positive since 10000 BC and lasted almost 7500 years, then gradually decreased to negative in 2500 BC to 1500 AD, and finally sharply increased to positive. The anomaly areas of the ND field in East Asia took shape for n = 3, when the anomaly areas in East Asia were shaped into closed circles in the mainland. This suggests that the first three harmonic degrees account for most of the ND field. The energy of the ND field rapidly attenuates at the core–mantle boundary and is stable at the surface.
Keywords: geomagnetic field, nondipole, CALS10K.1b, IGRF11

Introduction

The geomagnetic field is defined as the magnetic field that is produced by all sources within and outside the solid Earth up to the magnetosphere (Hulot et al., 2007). The variation of the geomagnetic field ranges from seconds to thousands of years. Short-term variations are mainly caused by external disturbances, i.e., ionospheric and magnetospheric, and solar activities, whereas long-term variations are mainly internal. Understanding the spatiotemporal variation of the global geomagnetic field in long timescales allows us to understand movements in the core (Wardinski and Korte, 2008) and the relation between magnetic field and physical processes, e.g., the geodynamo process.

The nondipole (ND) magnetic field can be obtained after removing the geocentric dipole field from the main field and occupies about 10% of the total geomagnetic field intensity. Empirical models are generally used to analyze the spatiotemporal variations of the ND field. The models systematize secular variations of the geomagnetic field. The ND field is also very important in many geophysical applications, such as

Manuscript received by the Editor December 25, 2015; revised manuscript received April 5, 2017.
*This work was supported by the National Natural Science Foundation of China (Grant No. 41404053) and the Natural Science Foundation of Jiangsu Province, China (Grant No. BK20140994).
1. The College of Mathematics and Statistics, Nanjing University of Information Science & Technology, Nanjing 210044, China.
2. State Key Laboratory of Space Weather, Chinese Academy of Sciences, Beijing 100080, China.
♦Corresponding author: Feng Yan (Email: frank_feng8848@163.com)

investigations of westward and eastward movements of the core (Dumberry and Bloxham, 2006; Dumberry and Finlay, 2007; Wardinski and Korte, 2008), field asymmetries related to archeomagnetic jerks (Gallet et al., 2009), and age constraints for archeological stratigraphic applications (Korte et al., 2011). Bauer (1899) studied the ND field for the first time; hitherto, significant studies of the ND field in different scales have been published (Baag and Helsley, 1974; Walker and Backus, 1997; Feng et al., 2014). However, there are shortcomings, such as the low resolution of global models and the uneven distribution of survey data. These shortcomings produce differences among the different global models. With improvements in data collection and modeling techniques, several high-resolution, and highly precise models have been published, such as the comprehensive model (Langel et al., 1996; Sabaka et al., 2002, 2004, 2015) and the CHAOS model (Olsen et al., 2006, 2009, 2010, 2015; Olsen and Mandea, 2008). However, the timescales of these models range from tens to hundreds of years, producing large-scale uncertainties in geomagnetic field modeling.

For long timescales, Bloxham and Jackson (1992) created the continuous UFM1 and UFM2 models for the magnetic field between 1840 AD and 1990 AD and 1690 AD and 1840 AD, respectively. They also derived a magnetic field model for the core–mantle boundary (CMB) for 1715 AD to 1980 AD (Bloxham and Gubbins, 1985). Jackson et al. (2000) created the continuous GUFM1 model, based on historical data for 16th-century declination and inclination, which covers the years 1590 AD to 1990 AD. Constable et al. (2000) derived a global snapshot model by combining datasets of archeomagnetic and paleomagnetic data for the last 3000 years. Subsequently, Korte and Constable (2003) derived a continuous archeomagnetic and lake sediment geomagnetic model for the last 3000 years (CALS3K.1) based on the same dataset, which covered 24 global sites with a maximum deviation of 10° from the present-day geomagnetic field but without small-scale structure owing to uneven distribution of the data. The 2005 version, CALS7K. 2 (Korte and Constable, 2005), is able to estimate the geomagnetic field of the last 7000 years starting in 5000 BC. In 2011 the CALS3K.4 (3K.4) and CALS10K.1b (10K.1b) models were derived (Korte and Constable, 2011; Korte et al., 2011). The CALS10K.1b (10K. 1b) model is the first time-varying spherical harmonic geomagnetic field model that spans 10000 years. Compared with earlier CALSxK models, the 10K.1b version covers longer periods (10000 BC to 1990 AD) and is more reliable owing to the inclusion of numerous intensity data from sediments. It is suggested that predictions prior to 7000 BC are less certain owing to the smaller data population.

Despite several studies on the global and regional ND field (Lin et al., 1985; Yukutake and Tachinake, 1969; Kang et al., 1995; Feng et al., 2014), spatiotemporal studies of the Chinese mainland that cover more than 10000 years are rare. This study is concerned with the spatial and temporal variations of the ND field over China from 10000 BC to 1990 AD; moreover, the magnetic anomaly in East Asia and the contributions of different ND field sources are also investigated to understand the geophysical features of the ND field. All studies mainly use the time-dependent 10K.1b geomagnetic model. To verify and study the variation of the ND field and its energy, especially after 2000 BC, we compare results using the 3K.4 and IGRF11 models. Considering the radial component (Z) throughout the core, CMB, and surface, we reflect on the intensity variations of the deep interior, especially at the CMB.

Data and methods

Data

Two kinds of data were adopted to derive the 10K.1b model. Data from 75 sites of rapidly accumulated sediments that preserve the postdepositional magnetic remanence were considered. In addition, materials with thermal remanent magnetization, i.e., archeomagnetic data were selected (Korte et al., 2011). To derive the model, data from six sites were used. The data contain intensity variations, and the archeomagnetic data were from the GEOMAGIA v.2 dataset (Donadini et al., 2009; Korhonen et al., 2008) and include individual directional and absolute paleointensity data as well as age and uncertainty data. About 80% of the data covered the last 3000 years.

The dataset of the 3K.4 model was based on the same data compilations as 10K.1b (Korte and Constable, 2011). For IGRF11, which was based on the latest satellite observations, magnetic observatories, and magnetic surveys (Finlay et al., 2010), the time range was 1900 AD to 2010 AD.

Methods

The modeling principles of 10K.1b and 3K.4 are the same. The regularized modeling method that is based on the conventional spatial expansion in spherical harmonic functions and the temporal expansion in cubic B-spline

functions was chosen (Korte and Constable, 2011). The actual spatial and temporal resolution is reliable because of the data quality and distribution. By considering an insulated mantle and ignoring the crustal and external fields, the time-dependent geomagnetic field B can be expressed by the negative gradient of the scalar potential V, $B = -\nabla V$, outside the Earth's core. V is a classical spherical harmonic function.

Following earlier CALSxK models, the spatial basis functions were expanded up to a maximum degree of ten. The number of B-splines increased to provide a knot-point spacing of 40 years, and iterative linear inversion was adopted to fit the data.

For smooth fitting, the physically motivated regularization norm was adopted at the CMB, by which the lower bound on ohmic dissipation (Gubbins, 1975) is minimized. Then,

$$\psi = \frac{4\pi}{t_e - t_s}\int_{t_s}^{t_e} f(B_r)\mathrm{d}r, \tag{1}$$

where t_s, t_e are the start and end time points and $f(B_r)$ is the quadratic norm associated with minimum ohmic heating of the field and is represented by spherical coefficients

$$f(B_r) = \sum_{n=1}^{N}\frac{(n+1)(2n+1)(2n+3)}{n}\left(\frac{a}{c}\right)^{2n+3} \cdot\sum_{m=0}^{n}[((g_n^m(t))^2 + (h_n^m(t))^2)], \tag{2}$$

In equation (2), a is the mean radius of the Earth's surface (a = 6371.2 km), r is the radial distance, $c = r$, B_r is the radial element, g_n^m and h_n^m are the Gauss coefficients, and N is the maximum harmonic degree

After decomposing the geomagnetic field in spherical center coordinates, we obtain

$$B_r = -\sum_{n=1}^{10}\sum_{m=0}^{n}(n+1)\left(\tfrac{a}{r}\right)^{n+2}(g_n^m(t)\cos m\lambda + h_n^m(t)\sin m\lambda)P_n^m(\cos\theta). \tag{3}$$

For the temporal part, the temporal norm of the minimum surface integral of the second derivative of the radial field is

$$\Lambda = \frac{4\pi}{t_e - t_s}\int_{t_s}^{t_e}\int_{CMB}(\partial_t^2 B_r)^2\,\mathrm{d}\Omega\mathrm{d}t, \tag{4}$$

The measured directional and intensity data are nonlinearly related to the coefficients that are obtained iteratively. Based on the functions above, the ND field is obtained by setting coefficients that correspond to n = 1 as 0.

For IGRF11, the modeling principles are almost the same as in 3K.4, except for the regularization. In addition, to compare and study the ND field of the three models, the maximum degree of IGRF11 was set at 10. In all, 120 coefficients were obtained from http://earthref.org and http://www.ngdc.noaa.gov/IAGA/vmod/igrf.html.

Results

Spatial and temporal variation of the ND field

To analyze Z of the ND field from 10000 BC to 1900 AD, we plotted 120 contour figures for every 100 years and compared them. According to the distribution in each epoch, the spatial variation of the ND field was divided into three periods. From 10000 BC to 2500 BC, the positive areas dominated the entire mainland and lasted for 7500 years. From 2500 BC to 1500 AD, the intensity of the ND field gradually decreased, and positive areas changed to negative for 4000 years. Finally, from 1500 AD to 1900 AD, the intensity increased, and negative areas turned positive.

To show the main temporal variations, we used the mean intensity variation for 100 years.

Figure 1 shows the mean intensity of Z oscillating between 0 and 50 nT and 10000 BC and 3000 BC. Since 3000 BC, the intensity has been decreasing continuously and reached −60 nT/a in 0 AD, then gradually increased from 0 AD to 1900 AD, and finally reached more than 100 nT/a. The intensity increased 105.01 nT/a during the entire period and is 13.73 times the original value in 10000 BC. Although the mean values do not precisely reflect amplitude variation owing to the inevitable offset of positive and negative values, they roughly correspond to the three periods mentioned above.

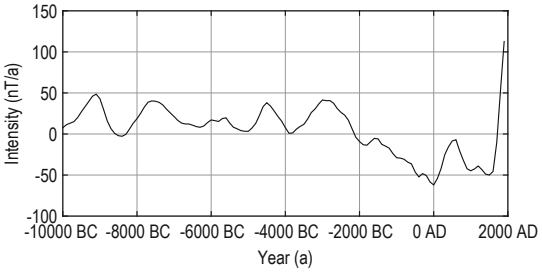

Fig.1 Mean variation of Z of the ND field in the Chinese mainland based on the 10K.1b model from 10000 BC to 1900 AD.

The generation of a strong ND anomaly over East Asia is noteworthy. Yukutake (1969) argued that the ND anomaly over East Asia occurred 400 years ago. To check this, we derived the yearly distribution from 1600 AD to 1700 AD and found that the anomaly originally emerged in 1682 AD (Table 1), 90 years earlier than that derived by Yukutake (1969). The difference is attributed to the use of different datasets. The new results are more reliable owing to the high quality of the latest dataset. The extreme intensity of the anomaly increased from 80.69 nT to 18209.42 nT from 1682 AD to 1990 AD and finally to 18128.73 nT. The latitude and longitude of the extremes moved 8.3° southward and 11.3° eastward since 1682 AD, and the location of the extremes keeps moving into the southeast mainland. There is almost no obvious relation between the attenuation of the dipole moment of the ND field and the change of the ND field over East Asia (Kang et al., 1995). In addition, the anomaly shape of the 2^n ($n > 1$) ND field has the same origin as the East Asia anomaly and corresponds to the long wavelengths; moreover, this originated from deeper in the Earth.

Table 1 Location and intensity of the extreme magnetic anomalies in East Asia

Year	Latitude (°)	Longitude (°)	Intensity (nT)
1682 AD	52.3	91.4	80.69
1700 AD	51.8	104.6	1419.35
1800 AD	48.9	106.6	8789.94
1900 AD	42.9	106.6	15328.36
1990 AD	44.0	102.7	18209.42

To verify the model, we compare the ND field of Z for the 10K.1b, 3K.4, and IGRF11 models after 1900 AD at intervals of five years (Figure 2).

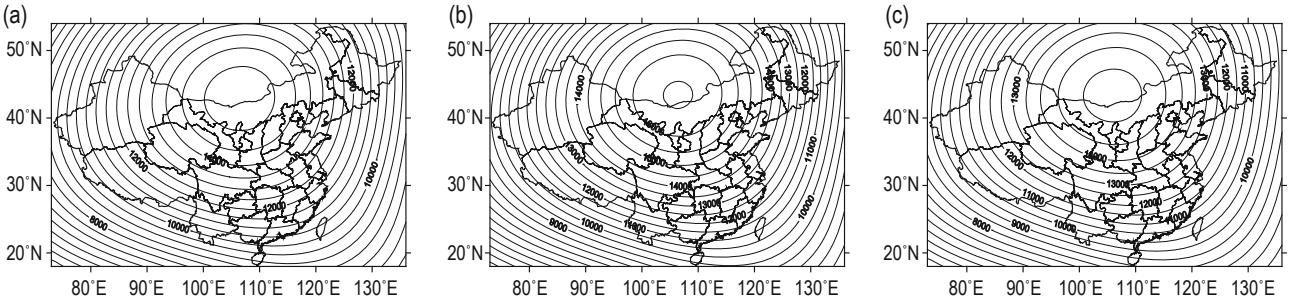

Fig.2 Distribution of anomalies over East Asia in 1900 AD: (a) CALS10K.1b; (b) CALS3K.4; (c) IGRF11.

The distributions are consistent with the Lin et al. (1985) study. To further examine the results, we look at the variation of latitude and longitude, and the anomaly intensity of the extremes over East Asia with time.

According to Figure 3, the location change of the extremes is very small. The latitude of the extremes in 3K.4 and IGRF11 is different from that in 10K.1b. The latitude first moves southward and then northward, whereas for 10K.1b it has been moving northward since 1900 AD. The latitude for 3K.4 and IGRF11 is at 42.9° around 1930 AD and at 44.3° in 1955 AD, whereas that for 10k.1b oscillates between 43.1° and 43.9° from 1900 to 1960 AD and keeps moving northward from 1960 AD. The latitude in IGRF11 moves southward from 1990 AD to 2010 AD. The annual rate of change of the latitude in the 10K.1b, 3K.4, and IGRF11 models is 0.012, 0.008, and 0.001°/a, respectively. The longitude change of the extremes in the three models is basically the same. It first moves westward from 1900 AD and eastward from 1980 AD, and then continuously drifts westward after reaching around 103.3° in 1995 AD according to IGRF11. The annual rate of change of longitude of the three models is −0.043, −0.039, and −0.040°/a, respectively. The intensity of the extremes increases

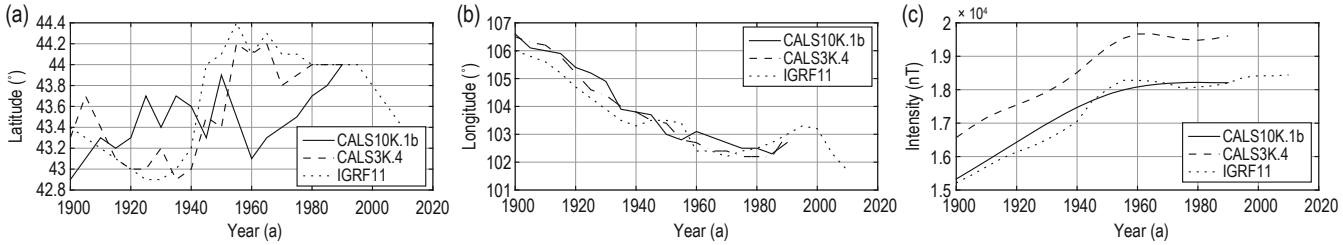

Fig.3 Variation of latitude (a), longitude (b), and intensity (c) of the ND extremes from 1900 AD to 1990 AD.

nearly linearly with time. The variation of 3K.4 and IGRF11 is the same, whereas that of 10K.1b is smoother and changes linearly and that of 3K.4 is higher than the other two models and around 1000 nT. The intensities of 10K.1b, 3K.4, and IGRF11 change from 15328.36, 16569.59, and 15212.89 nT to 18209.42, 19608.67, and 18476.49 nT, respectively, with annual change rates of 32.01, 33.78, and 29.70 nT/a, suggesting increasing intensity for the 10K.1b and 3K.4 models and faster than IGRF11.

Field source

Based on spherical harmonics, different degrees of spherical harmonic models have specific geophysical meaning, such as magnetic field caused by field sources at different depths. To better demonstrate the intensity and distribution of the ND field that corresponds to each degree, we separately computed and drew the ND field of Z at different degrees (n = 2–10) for the three models. The results suggest that the shapes remain the same with increasing n. As the coefficients of the different degrees reflect the different wavelengths of the geomagnetic field, the high-degree coefficients are powers of the short wavelength and vice versa. The distributions of the ND field for the three models take shape at n = 3, when the anomalies in East Asia form closed circles inside the northwestern mainland, and have the same origin as the East Asia anomaly; moreover, they originate from deeper in the Earth (see also Kang, 1995). The shape of the anomaly distribution is similar for n > 4. Table 2 lists the location and intensity extremes of the model anomalies at different n values.

Table 2 Location and intensity extremes for the three models at different n

Degree (n)	IGRF11			CALS10K.1b			CALS3K.4		
	Latitude (°)	Longitude (°)	Z (nT)	Latitude (°)	Longitude (°)	Z (nT)	Latitude (°)	Longitude (°)	Z (nT)
2	54.0	124.2	12273.99	54.0	124.7	12291.04	54.0	124.9	13095.4
3	42.3	90.7	14526.29	42.3	90.9	14535.66	42.1	90.3	15570.03
4	40.8	97.4	17912.86	40.9	97.2	17923.69	40.9	97.4	19288.44
5	41.5	99.1	18038.86	41.7	98.5	18060.83	41.3	99.1	19443.76
6	43.9	102.3	18594.7	43.7	101.9	18622.68	43.9	102.2	20082.91
7	43.7	102.5	18154.2	43.4	102.9	18176.5	43.8	102.5	19572.14
8	44.3	103.3	18240.32	44.4	103.5	18276.46	44.3	103.7	19690.8
9	43.9	102.9	18220.88	43.6	102.6	18235.84	43.9	103.2	19641.66
10	44.0	103.0	18201.58	43.6	102.6	18210.33	44.1	103.4	19610.1

The data in Table 2 suggest that the extreme locations of the anomaly for the three models are almost the same for n = 2. The intensities of IGRF11 and 10K.1 are around 12200 nT, whereas the intensity of 3K.4 is around 13000 nT. The extreme locations of the three models are nearly fixed at around 44°N and 103°E for n > 5, and the intensities are around 18200 and 19600 nT. The location is highly consistent among the three models, and the extreme locations of the anomaly move slightly northeast. The intensity continuously increased around 6000 nT with increasing n.

Each degree of the spherical harmonic coefficients has its own geophysical implications (Xu, 2003). To further compare and analyze, we calculated the 22, 23 … and 210 pole fields. The resulting distributions are significantly consistent, and the distribution of the 2^n pole field is mainly positive inside the mainland for n = 2–4 and becomes almost negative for n = 5–8. The distribution finally becomes positive at n > 8. Overall, the intensities in the mainland slowly decrease with increasing n.

Energy is another geophysical index of the ND field. To observe the energy variation of each 2^n pole field, the ND field energies of Z at the surface and CMB were computed. The energy of the geomagnetic field is generally expressed as

$$E(b,c,t)=\frac{1}{2\mu_0}\int_b^c\int_0^\pi\int_0^\pi B^2(r,\theta,\lambda,t)r^2\sin\theta\mathrm{d}\theta\mathrm{d}\lambda\mathrm{d}r, \quad (5)$$

where B is the intensity of the magnetic field, r, θ, λ are the radial distance, colatitude, and longitude, μ_0 is the vacuum permeability, and $b < r < c$. Because of the orthogonality of associated Legendre polynomials, the energies of X, Y, Z, and the total energy are obtained. The energy of Z is

$$E_z(b,c,t) = \frac{2\pi a^3}{\mu_0}\sum_{n=1}^{N}\sum_{m=0}^{n}\frac{(n+1)^2}{(2n+1)^2} \cdot[(\frac{a}{b})^{2n+1} - (\frac{a}{c})^{2n+1}][(g_n^m)^2 + (h_n^m)^2]. \quad (6)$$

To precisely study the energy of the $2n$ (n = 2–10) pole fields, we plotted the ND field energy of Z from 10000 BC to 1990 AD (IGRF11 is from 1900 AD to 1990 AD) at the surface and CMB.

From 10000 BC to 2000 BC, the energy of the ND field for the 10K.1b model first increases up to 6200 BC and reaches 1.3 × 10^{17} J at the surface and 4.9 × 10^{17} J at the CMB, and then gradually decreases. From 2000 BC, the energy trends for the 10K.1b and 3K.4 models at the surface and CMB are consistent, except for 800 AD to 1200 AD, whereas the energy of the 10K.1b model decreases and that of 3K.4 increases. Clearly, the energy of 3K.4 is higher than that of 10 K.1b at the surface and CMB. From 1900 AD, the variation of the three models is consistent, which implies that the variations derived from 10K.1b and 3K.4 are reliable. The trend of 3K.4 is closer to that of IGRF11 and is slightly smaller than that of 10K.1b. Based on the change of energy between the surface and the CMB, the energy attenuates rapidly at the CMB but slowly at the surface.

We used 10K.1b and IGRF11 to compare the change in energy. Figures 4 and 5 show that the energy of the 2^n pole field for IGRF11 and 10K.1b is greater at the CMB than at the surface by more than one order of magnitude. The amplitude of the attenuation at each 2^n pole field at the CMB is 94.66%, 96.72%, 98.12%, and 99.39% with increasing n.

In addition, the attenuation of energies for different n values in IGRF11 and 10K.1b suggests that the rate of the attenuation of the high-degree pole fields is $(a/r)^{n+2}$ with depth. The results suggest that the mean attenuation increases for n = 3 and 4 faster than the other pole fields. Variations of the 26–210 pole fields at the CMB oscillate relative to the surface. According to Gubbins and Herrero-Bervera (2007), the dynamo in the Earth's core represents the dipole of the geomagnetic field (the largest part), whereas the other is the Earth's lithosphere. The results also suggest that the energies of the low-degree (n = 2–5) pole fields at the CMB are very close, and the energy here rapidly decreases but the energy of the high-degree (n > 5) pole fields slowly decreases.

The main sources of the lithospheric magnetic field are magnetic rocks, relatively close to the surface and stable. The source intensities of the high-degree (n = 6–10) pole fields are somewhat affected by the lithospheric field and consequently cause the attenuation to oscillate. In summary, the energies of the higher degree ND pole fields attenuated about 99% compared with those at the CMB, and the attenuation speeds of lower degree ND pole fields are faster than those of the high-degree pole fields.

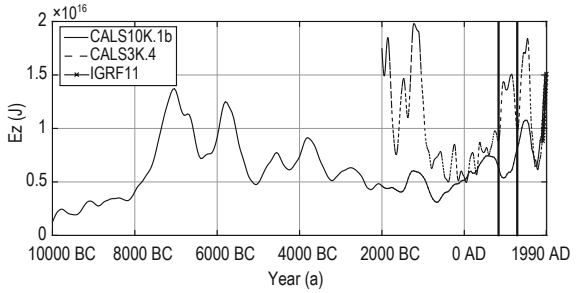

Fig.4 ND field energy of Z at the surface based on the three models for 10000 BC to 1990 AD.

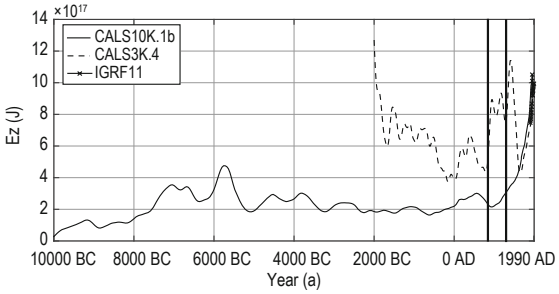

Fig.5 ND field energy of Z at the CMB based on the three models for 10000 BC to 1990 AD.

Conclusions

We combined the global geomagnetic field model CALS10K.1b with the CALS3K.4 and IGRF11 models, and analyzed the ND field of Z at different intervals and the distribution of 2^n pole fields and their corresponding energies at the surface and CMB.

There are three main variation periods of the ND field in the Chinese mainland and neighboring regions from 10000 BC to 1900 AD. The regional intensity of the ND field decreased from positive between 10000 BC and 2500 BC to negative between 2500 BC and 1500 AD, and after 1500 AD increased to positive. The magnetic anomaly of ND over East Asia originally occurred in 1682 AD. The anomaly intensity gradually increased until 1900 AD, and the intensity of this extreme point increased nearly linearly whereas the location of this

extreme point moved southeast.

The ND field of the three models basically took shape for n = 3, when the anomaly areas in East Asia were shaped as closed circles inside the mainland. This implies that the first three degrees of the ND field for n =1–3 account for most of the ND field. The extreme locations of the anomaly are almost the same for the three models for n = 2 and then move northeast in the mainland.

The field source energies change trends at the surface and CMB similarly, except for the difference from 800 AD to 1200 AD. In the study period, the energy rapidly attenuated from the CMB but remained stable at the surface. The amplitude of the attenuation at each 2^n pole field at the CMB was 94.66%, 96.72%, 98.12%, 99.39%, and higher with increasing n. The energies for n = 2–5 significantly decreased with increasing depth of the outer liquid core but the intensities remained stable for n = 6–10, which implies that the low-degree ND field over China and the neighboring regions may have a deeper source.

We compared the distribution and intensity of the 3K.4, IGRF11, and 10K.1b models. Even though the results are reliable, there is still room for improvement. The spatial and temporal variations of the ND energy from 800 AD to 1200 AD, and the shape and movement of the magnetic anomaly of ND over East Asia help us to understand the distribution and variation of the ND field over the Chinese mainland from 10000 BC to 1990 AD. In addition, the 10K.1b model provides valuable information regarding the ND field in millennial scale.

The dipole moment decreased during the last several thousand years. In particular, during the last 180 years, the intensity of the dipole field has decreased around 10%, which denotes geomagnetic field reversal. However, the ND field, especially Z, has been increasing during this period, which suggests that it does not synchronously change between the dipole field and the ND field. Moreover, this phenomenon implies that the ND field is important during geomagnetic field reversal. Although the proposed physical explanation for the ND field is not impressive, it may help theoretical geophysical studies and can have practical applications like mineral exploration and mining, etc.

Acknowledgments

We acknowledge the support of the State Key Laboratory of Space Weather, Chinese Academy of Sciences and the Jiangsu Government Scholarship for Overseas Studies. We also thank the reviewers for valuable advice.

References

Baag, C., and Helsley, C., 1974, Geomagnetic secular variation model: Journal of Geophysical Research, **79**(32), 4918−4922.

Bauer, L., and Hazard, D., 1900, The physical decomposition of the earth's permanent magnetic field-No. 1. the assumed normal magnetization and the characteristics of the resulting residual field: Terrestrial Magnetism and Atmospheric Electricity, **5**(1), 1−4.

Bloxham, J., and Gubbins, D., 1985, The secular variation of earth's magnetic field: Nature, **317**, 777−781.

Bloxham, J., and Jackson, A., 1992, Time-dependent mapping of the magnetic field at the core-mantle boundary: Journal of Geophysical Research, **97**(B13), 19537−19563.

Constable, C., Johnson, C., and Lund, P., 2000, Global geomagnetic field models for the past 3000 years: transient or permanent flux lobes: Philosophical Transactions of The Royal Society A, **358**(1768), 991−1008.

Donadini, F., Korte, M., and Constable, C., 2009, Geomagnetic field for 0–3 ka: 1. New data sets for global modeling: Geochemistry Geophysics Geosystems, doi:10.1029/ 2008GC002295.

Dumberry, M., and Bloxham, J., 2006, Azimuthal flows in the earth's core and changes in length of day at millennial timescales: Geophysical Journal International, **165**, 32–46.

Dumberry, M., and Finlay, C., 2007, Eastward and westward drift of the earth's magnetic field for the last three millennia: Earth and Planetary Science Letters, **254**, 146–157.

Feng, Y., Jiang, Y., and Sun, H., et al., 2014, A Study on variations of non-dipole magnetic field over Chinese mainland during 2000BC to 1990 AD: Science China (Earth Science), **57**(6), 1229−1244.

Finly, C., Maus, S., Beggan, C., et al., 2010, International geomagnetic reference field: the eleventh generation: Geophysical Journal International, **183**(3), 1216–1230.

Gallet, Y., Hulot, G., Chulliat, A., et al., 2009, Geomagnetic field hemispheric asymmetry and archeomagnetic jerks: Earth and Planetary Science Letters, **284**, 179–186.

Gubbins, D., 1975, Can the Earth's magnetic field be sustained by core oscillations? Geophysical Research Letters, **2**(9), 409−412.

Gubbins, D., and Herrero-Bervera, E., 2007, Encyclopedia of geomagnetism and paleomagnetism: Springer, Netherlands.

Hulot, G., Sabaka, T., and Olsen, N., 2007, Treatise on Geophysics, Geomagnetism. Amsterdam: Elsevier Ltd.

Jackson, A., Jonkers, A., and Walker, M., 2000, Four centuries of geomagnetic secular variation from historical records: Philosophical Transactions of The Royal Society A, **358**(1768), 957–990.

Kang, G., Yu, H., and Zhang, Z., 1995, Change characteristics of geomagnetic the non-dipole field in east Asia: Journal of Yunnan University (in Chinese), **17**(4), 358–368.

Korhonen, K, Donadini F, and Riisager, P., 2008, Geomagia 50: An archeointensity database with PHP and MySQL. Geochem Geophys Geosys, **9**, 9Q04029, doi: 10.1029/2007GC001893.

Korte, M., and Constable, C., 2003, Continuous global geomagnetic field models for the past 3000 years. Physics of the Earth and Planetary Interiors, **140**(1–3), 73–89.

Korte, M., and Constable, C., 2005, Continuous geomagnetic field models for the past 7 millennia: CALS7K. 2: Geochemistry Geophysics Geosystems, doi: 10.1029/2004GC000801.

Korte, M., and Constable, C., 2011, Improving geomagnetic field reconstructions for 0–3 ka: Physics of the Earth and Planetary Interiors, **188**(3–4), 247–259.

Korte, M., Constable, C., Donadini, F., and Holme, R., 2011, Reconstructing the holocene geomagnetic field: Earth and Planetary Science Letters, **312**(3–4), 497–505.

Langel, R., Sabaka, T., Baldwin, R., et al., 1996, The near Earth magnetic field from magnetospheric and quiet-day ionospheric sources and how it is modeled: Physics of the Earth and Planetary Interiors, **98**(3–4), 235–267.

Lin, Y., Zeng, X., and Guo, Q., 1985, Analysis of secular variation of non-dipole geomagnetic field in eastAsia. Chinese Journal of Geophysics (in Chinese), **28**(5), 482–496.

Olsen, N., Hulot, G., Lesur, V., et al., 2015, The Swarm Initial Field Model for the 2014 geomagnetic field: Geophysical Research Letters, **42**, DOI 10.1002/2014 GL062659.

Olsen, N., Luhr, H., Sabaka, T., et al., 2006, CHAOS—a model of Earth's magnetic field derived from CHAMP, Oersted, and SAC-C magnetic satellite data: Geophysical Journal International, **166**(1), 67–75.

Olsen, N., and Mandea, M., 2008, Rapidly changing flows in the Earth's core: Nature geosciences, **1**, 390–394.

Olsen, N., Mandea, M., Sabaka, T. J., et al., 2009, CHAOS-2—a geomagnetic field model derived from one decade of continuous satellite data: Geophysical Journal International, **179**(3),1477–1487.

Olsen, N., Mandea, M., Sabaka, T., et al., 2010, The CHAOS-3 geomagnetic field model and candidates for IGRF-2010: Earth Planets Space, **62**, 719–727.

Sabaka, T., Olsen, N., and Langel, R., 2002, A comprehensive model of the quiet-time, near-Earth magnetic field: phase 3: Geophysical Journal International, **151**(1), 32–68.

Sabaka, T., Olsen, N., and Purucker, M., 2004, Extending comprehensive models of the earth's magnetic field with Oersted and CHAMP data: Geophysical Journal International, **159**(2), 521–547.

Sabaka, T., Olsen, N., Robert H., et al., 2015. CM5, a pre-Swarm comprehensive geomagnetic field model derived from over 12 yr of CHAMP, Ørsted, SAC-C and observatory data: Geophysical Journal International, **200**, 1596–1626.

Walker, A., and Backus, G., 1997, A six-parameter statistical model of the earth's magnetic field: Geophysical Journal International, **130**(3), 693–700.

Wardinski, I., and Korte, M., 2008, The evolution of the core-surface flow and changes in the length of day over the last seven thousand years: Journal of Geophysical Research, doi:10.1029/2007JB005024.

Xu, W., 2003, Geomagnetism. Beijing: Earthquake press.

Yukutake, T., and Tachinake, H., 1969, The non dipole part of the earth's magnetic field into drifting and standing parts: Bull. Earthquake Res. Inst., **47**, 65–79.

Feng Yan, Ph.D. is presently working at the College of Mathematics and Statistics, Nanjing University of Information Science & Technology. His research interests include modeling of the regional and global geomagnetic field, geomagnetic field secular variations, and the relation between geomagnetic field and space weather.

Cell-phone: 13655187350